

MAŁGORZATA SKORUPA *, ADAM KORBEL*

MODELLING THE SECONDARY BENDING IN RIVETED JOINTS WITH ECCENTRICITIES

For riveted joints with eccentricities of the load path, bending moments referred to as secondary bending are induced under nominally tensile loading conditions. Two simple theoretical models proposed in the literature to estimate the associated bending stresses are evaluated in the paper. Both approaches have been implemented in computer programs and applied to estimate the effect of several variables on the calculated bending stresses in the lap joint. Possibilities of the experimental and numerical verification of the models are also considered. Finally, a correlation between the secondary bending computed by one of the simple models and the observed fatigue properties of riveted specimens, as reported in the literature, is investigated. It is shown that deviations of the experimental results from the theoretical expectations stem from additional to secondary bending factors, like the inhomogeneous load transmission through the joint and the residual stresses induced by riveting process. These phenomena are known to be relevant to the fatigue behaviour of riveted joints, but they are not accounted for by the simple models. A conclusion from the present study is that despite the limitations and approximations inherent in the simple models, they provide reliable estimates of nominal bending stresses at the critical rivet rows and can be utilized in currently used semi-empirical concepts for predictions on the fatigue life of riveted joints.

1. Introduction

Riveting is one of the major methods for holding together sheet panels, stringers and stiffeners of the fuselage of an aircraft and its use will continue in the foreseeable future despite alternatives like welding and bonding. Among primary advantages of the riveted joints are their low production cost, utilization of conventional metal-working tools and techniques, possibility of the riveting process automation, ease of inspection, possibility of their repeated assembling and disassembling for the fabrication

* AGH University of Science and Technology, Al. Mickiewicza 30, 30-059 Kraków, Poland; E-mail: korbel@agh.edu.pl

replacement or repair, good hole filling properties of the rivets and, last but not least, a long-standing experience of the industry with riveted joints. At the same time, however, the riveted joints represent a fatigue critical element in metallic airframe construction. For example, the present problem of aging aircraft is associated with fatigue of riveted lap joints in pressurized fuselage structure [1]. Understanding the fatigue process within riveted joint requires a detailed knowledge of the local stress state. The local stresses are affected by factors associated with high stress concentration at the rivet hole, the load transfer through the rivet and the rivet installation. The rivet installation process imparts residual stresses in the vicinity of the holes. Another result of rivet installation are frictional forces between the mating sheets induced due to the clamp-up which contribute to fretting damage at the faying surface. For riveted joints with eccentricities of the load path, bending stresses which occur under a nominally tensile loading on the joint must also be considered. Bending caused by the tensile load on the joint is referred to as secondary bending. Crack path eccentricities are inherent in riveted joints typically present in aircraft fuselages, namely longitudinal lap joints and circumferential single strap joints.

The contribution of secondary bending is often quantified by the bending factor defined as

$$k_b = \frac{S_b}{S} \quad (1)$$

where S_b is the maximum nominal* bending stress, and S is the nominal tensile stress applied to the joint. Both S_b and S are computed for the gross section of the sheet, i.e. neglecting the rivet holes.

Maximum bending moments occur at eccentricities, namely at the fastener rows. For a lap joint with more than two rivet rows, the location of the maximum bending moments is always at the outer rows, i.e. row I and III for a most common configuration with three rivet rows shown in Fig. 1. Due to the deformation of the joint also depicted in Fig. 1, the nominal bending stresses adopt the highest positive value at location A of sheet 1 and location B of sheet 2. Their value is given by

$$S_{b,i} = \frac{6M_{b,i\max}}{Bt_i^2} \quad (2)$$

* Nominal stress is computed for the cross section neglecting the stress concentration.

where subscript i indicates the critical location (in sheet 1 or 2), $M_{b,i\max}$ is the maximum bending moment and B and t_i denote the specimen gross width and thickness respectively.

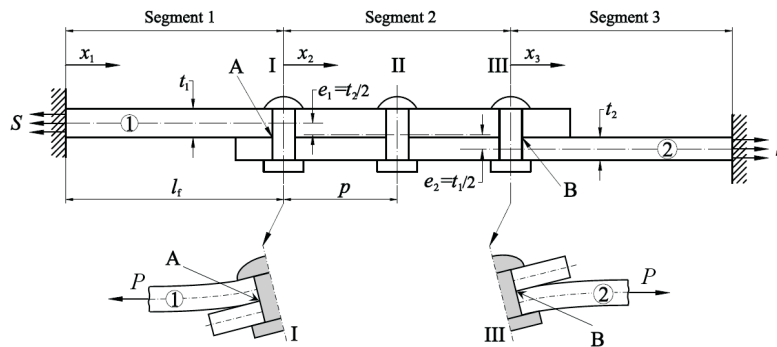


Fig. 1. Lap joint with three rivet rows

Because outside the overlap region either sheet carries the full load P coming from the pressurization of the fuselage, the maximum applied stresses equal

$$S_i = \frac{P}{Bt_i} \quad (3)$$

and, consequently, the maximum total nominal tensile stresses $(S + S_b)_i$ in the sheets also occur at A and B.

The nominal stresses due to the secondary bending can equal or even exceed the applied stresses. Fractographic investigations of riveted joints indicate that fatigue crack nucleation occurs at the sites of maximum bending stresses [2,3].

The subject of the present paper is modelling the secondary bending in riveted joint with eccentricities according to two simple theoretical concepts proposed in the literature [4,5]. Both approaches have been implemented in computer programs and applied to estimate the effect of several variables on the calculated bending stresses in the lap joint. Possibilities of the experimental and numerical verification of the models are also considered. Finally, a correlation between the secondary bending computed using the simple models and the observed fatigue properties of riveted specimens is investigated.

2. Simple models to estimate bending stresses in joints with eccentricities

In order to derive the bending moment at any site of a joint with eccentricities, the out of plane deformations of the sheets must be known. Concepts which enable to compute these deformations, represented by deflections of the joint neutral axis, have been proposed by Schijve [4] and Das et al [5]. Within the overlap, i.e. between the outer rivet rows, the sheets are assumed to act as a single integral beam, the flexural rigidity of which corresponds to the combined thickness of the sheets. The rivets itself are not modelled. The above simplifications imply that for a joint with more than two rivet rows, the presence of the inner rivet rows is not accounted for.

With both approaches referred to above, the joint is decomposed into segments of a constant flexural rigidity connected at the ends. As seen in Fig. 1, there are three segments in the case of a simple lap joint. From the theory of beams or flat shells under bending, the bending moment for segment i sketched out in Fig. 2 can be computed from the differential equation for the deflection $w_i(x_i)$ at any point x_i along the segment

$$M_{b,i}(x_i) = G_i w_i''(x_i) \tag{4}$$

with

$$M_{b,i}(x_i) = M_{i,A} + Vx_i + P[w_i(x_i) - w_i(0)], \quad i = 1 \text{ to } n \tag{5}$$

where V is the fixing reaction, G_i is the bending stiffness of segment i , $w_i''(x_i) = \frac{d^2 w_i(x_i)}{dx_i^2}$ and n is the number of the segments.

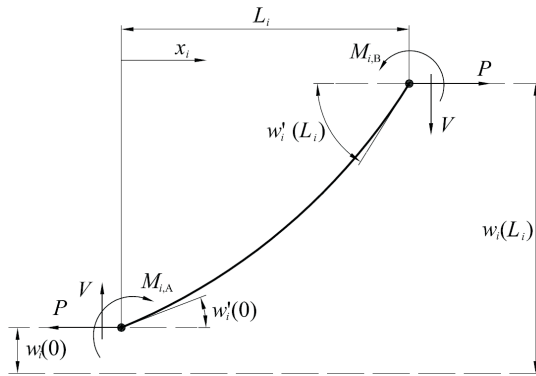


Fig. 2. Nomenclature for the calculation of the bending moment for segment i of a riveted joint

In the case of hinged clampings of the sheet ends, the fixing moments M_{1A} and $M_{n,B}$ and the reaction V equal zero.

The general solution of Eq. (4) is in the form

$$w_i(x_i) = A_i \cosh(\alpha_i x_i) + B_i \sinh(\alpha_i x_i) + C_i x_i + D_i \quad (6)$$

where:

$$\alpha_i = (P/G_i)^{1/2}, \quad C_i = -V/P \quad \text{and} \quad D_i = -M_{i,A}/P \quad (7)$$

The unknowns, namely the constants A_i , B_i , C_i and D_i , the reaction V and the moments $M_{i,A}$ can be solved by considering the equilibrium of the joint as a whole [4] or the equilibrium of the individual segments [5], and by setting the boundary conditions at the segment intersections and at the joint clamped ends, i.e. for $x_1 = 0$ and $x_n = L_n$. Matching the slopes at the intersection of segment i and $i+1$ is governed by the equation

$$w'_i(L_i) = w'_{i+1}(0) \quad (8)$$

where $w'_i(x_i) = \frac{dw_i(x_i)}{dx_i}$.

Though very much alike, the concepts of Schijve and Das et al differ, however, in some details. The effect of the joint eccentricities is covered in either model in a distinct way, as schematically shown in Fig. 3 for the case of a hinged (a) and rigid (b) clamping of the sheet ends. According to Schijve's approach, often referred to as the neutral line model, the neutral axis is stepped by the eccentricities between the segments both prior to and after the joint deformation. In case of eccentricity e_i between segment i and $i+1$ he assumes

$$w_{i+1}(0) = w_i(L_i) \pm e_i \quad (9)$$

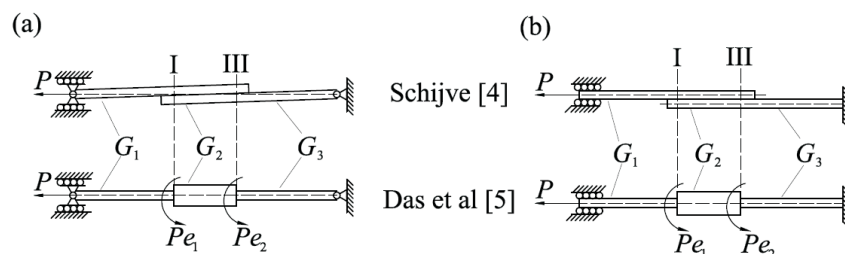


Fig. 3. Modelling the eccentricities for the lap joint from Fig. 1 according to [4] and [5] in case of hinged (a) and rigid (b) clamping of the sheet ends

Contrary to Schijve, Das et al consider $w(x)$ to be a continuous line which implies

$$w_{i+1}(0) = w_i(L_i) \quad (10)$$

and they account for the eccentricity by introducing an additional moment

$$M_{i+1,A} = M_{i,B} \pm Pe_i \quad (11)$$

Another difference between both concepts lies in covering the deflections in the overlap region. Schijve assumes that Eq. (4) holds also for segments between the outer rivet rows whilst Das et al consider these segments to be perfectly stiff. Thus, according to [5], if segment i represents the overlap region which is connected to segments $i - 1$ and $i + 1$, then

$$w_i(L_i) = w_i(0) + L_i w'_i(0) \quad (12)$$

and, consistent with Eq. (10),

$$w'_i(0) = w'_{i-1}(L_{i-1}) = w'_i(L_i) = w'_{i+1}(0) \quad (13)$$

To conclude the list of differences between both approaches, it should be mentioned that Schijve assumes plane stress conditions which implies the bending stiffness per unit width of

$$G_i = Et_i^3/12 \quad (14)$$

whilst plane strain conditions adopted by Das et al lead to

$$G_i = Et_i^3/[12(1 - \nu^2)] \quad (15)$$

where E is the modulus of elasticity and ν is Poisson's ratio.

3. Effect of the stress level and design variables on the amount of secondary bending in a lap joint

The models of Schijve [4] and Das et al [5] have been implemented in computer programs and used to quantify the influence of several variables on stresses induced by the secondary bending in the lap joint from Fig. 1. To solve Eq. (4) for $w(x)$, the joint has been divided into three segments, as shown in Fig. 1, the detailed derivation for Schijve's model being given elsewhere [6]. For the results presented in this section, equal thickness of both sheets are assumed, namely $t_1 = t_2 = t$.

The effect of the type of clamping the specimen ends on the model results is studied first. As pointed out by Schijve [4], the influence of clamping

conditions on the bending stress value can be avoided if the distance between the clamping edge and the outer rivet row (the so called free length l_f , Fig. 1) is sufficiently long. Müller [2] demonstrated numerically that for sheet thicknesses below 2 mm the minimum free length l_f of $50t$ suffices to make the change in the S_b value due to the change of the clamping conditions less than 1%. This is substantiated by the plots in Fig. 4 which present the sensitivity of the k_b -value to the type of clamping according to the model by Schijve [4]. It is seen in Fig. 4 that for a given sheet thickness the bending factor reaches a steady level at a certain limiting l_f/t -value which increases with t . A practical conclusion for laboratory fatigue tests is that in order to avoid the influence of the fixture type, much shorter specimens suffice in the case of thinner sheets compared to thicker sheets. The behaviour of model [5] is similar to that shown in Fig. 4.

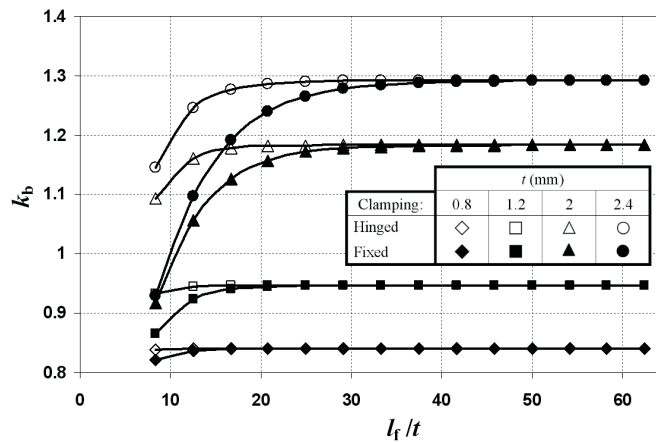


Fig. 4. Influence of the type of clamping the ends of the lap joint from Fig. 1 on the bending factor (k_b) depending on the sheet thickness (t) according to model [4].
The applied stress $S=100$ MPa

Plots in Fig. 5 demonstrate that the effect of secondary bending represented by the peak bending stress S_b and the bending factor k_b computed according to Schijve's model [4] becomes considerably reduced with decreasing the specimen thickness and with increasing the spacing p between the rivet rows. This could well be anticipated since thinner sheets imply smaller eccentricities and because for a longer p -distance the joint out-of-plane deflections are smaller. Note in Fig. 5 that S_b and, hence, also k_b are non-linear functions of the load on the joint and that the secondary bending is more severe at lower applied stresses S .

For the lap joint from Fig. 1, the largest deflections and, hence, the maximum bending moments occur at the end rivet rows, as already said earlier. This is correctly predicted by both models, as indicated in Fig. 6

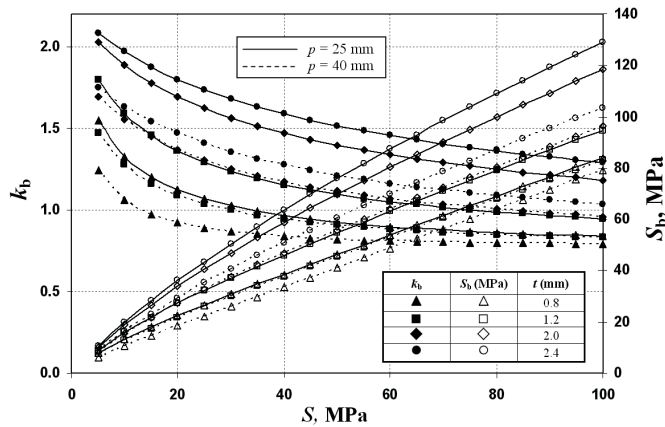


Fig. 5. Effect of the applied stress level (S), sheet thickness (t) and the rivet row pitch (p) on the bending factor (k_b) and the bending stresses (S_b) at the critical rivet rows for the lap joint from Fig. 1 according to model [4]

which shows variations of the bending stresses along the lap joint computed for two sheet thicknesses at the applied stress $S=120$ MPa. It is seen that for $t=2$ mm both solutions give very close results on the peak S_b -levels at the outer rivets (136 MPa [4] and 130.2 MPa [5]), whilst for $t=0.8$ mm the S_b -values differ quite significantly ($S_b=99.1$ MPa [4] and 66.5 MPa [5]). For $t=1.2$ mm the corresponding S_b values (not shown in Fig. 5 for clarity) are 109.9 MPa [4] and 91.3 MPa [5].

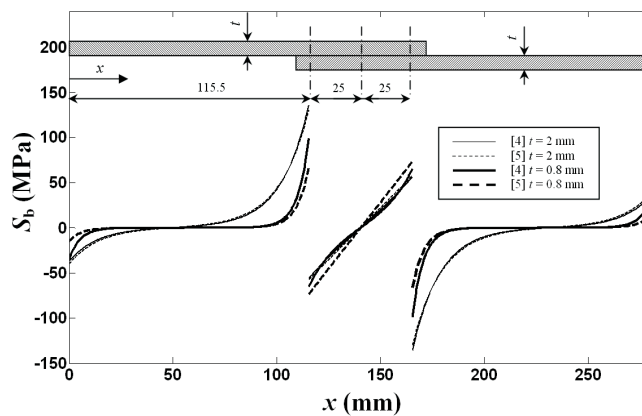


Fig. 6. Variations of the bending stresses along the lap joint according to model [4] and [5]. The applied stress $S=120$ MPa

Differences between the results from both models are further quantified in Figs. 7 and 8. In Fig. 7, $S_b[4]$ and $S_b[5]$ denote the peak bending stresses computed using the model of Schijve [4] and Das et al [5] respectively. Except at very low applied stresses, the $S_b[4]/S_b[5]$ ratio is above unity which

indicates that, generally, the model of Das et al yields lower estimates on S_b than the model of Schijve. The discrepancies become larger when the sheet thickness decreases, as already revealed in Fig. 6. Fig. 7 also demonstrates that for the very thin sheet of 0.8 mm in thickness the divergence in the results dramatically increases with increasing the S -level.

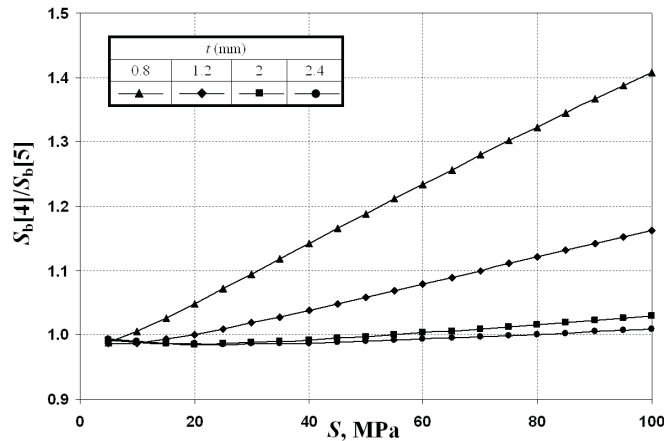


Fig. 7. Comparisons between the estimates of peak bending stresses for the lap joint from Fig. 1 according to model [4] and [5] for several sheet thicknesses. The rivet row spacing $p=25$ mm

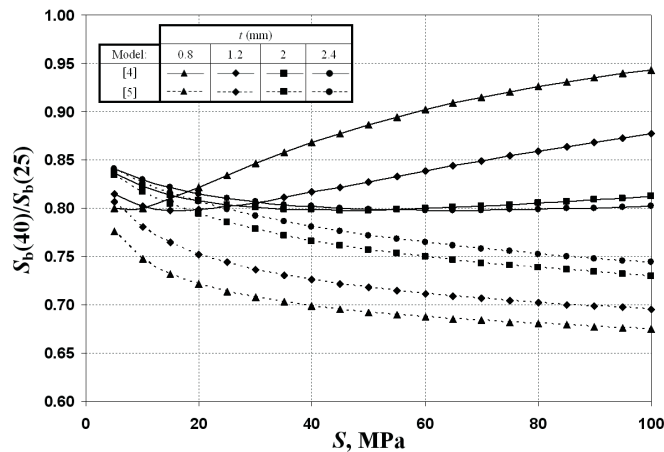


Fig. 8. Comparisons between the reduction in secondary bending due to increasing the rivet row spacing in the lap joint from 25 mm to 40 mm predicted according to [4] and [5] for several sheet thicknesses

Fig. 8 compares derived from both models estimate of the reduction in the peak bending stress for a range of the t -values due to increasing the spacing between the rivet rows. Here $S_b(40)$ and $S_b(25)$ denotes the bending stress at the critical location for the row spacing of 40 mm and 25 mm

respectively. Generally, compared to Schijve's model [4], Das et al [5] predict more benefits from increasing p , as evidenced by the plots according to [5] falling below those according to [4] except at very low S -levels. Interestingly, the results from either approach show a different behaviour with respect to S and t . According to Schijve, the effect of increasing p becomes weaker at higher applied stresses, whilst the reversed trend follows from the model of Das et al. Also, contrary to the latter approach, Schijve's model predicts the benefits of the larger p -distance to fade when the sheet thickness decreases. Consequently, in Fig. 8 the largest discrepancies in the $S_b(40)/S_b(25)$ ratio from both models are exhibited for the 0.8 mm thick sheet, whilst the differences for the thicker sheets (2 and 2.4 mm) are moderate.

The pronounced discrepancies in the results for thinner sheets revealed in the present study stem most probably from the distinct description of the overlap region deformation adopted in either model. Obviously, the lower is the sheet thickness, the more meaningful become differences between the deflections computed for the flexible (according to [4]) and the perfectly rigid (according to [5]) overlap. In the opinion of the present authors, disregarding the deformation of the overlap hardly has a physical foundation. Therefore, the model of Schijve [4] which does account for the overlap region deflection will be utilized in the analyses presented further on in this paper.

4. Verification of the simple models

An experimental or numerical verification of the models considered here is not straightforward. Experimental studies [2] and FE analyses [7] indicate that due to the presence of holes and the discrete load transmission through the rivets the stress distribution both along the joint width and along the rivet columns is highly non-uniform. The so called edge effect caused by differences in lateral contraction of the sheets in the overlap area can additionally contribute to the stress state inhomogeneity in the riveted joint. Because the above complexities are by assumption ignored in the one-dimensional models considered here, these approaches only enable estimates of the nominal stresses. Thus, it would not be appropriate to compare the S_b -stresses produced by the simple models with experimental or FEM results derived at locations close to the holes where a severe stress concentration occurs. For lap joint specimens with three rivet rows Rijck [8] noted a very good conformity of his strain gauge measurement results with the bending stresses computed by the model of Schijve [4]. The gauges were bonded along an inner rivet column outside the overlap area at a distance of half the rivet pitch from the outer rivet row. Within the overlap region where, however, the bending stresses are much lower (see Fig. 6), the com-

puted and measured data compared less favourably which can be attributed to neglecting in the model differences in the loads transmitted by the sheets within the overlap. Also, Brenner and Hübsch [9] reported a satisfactory agreement between the bending stresses computed for a single strap joint using a method similar to Schijve's model and those measured with strain gauges bonded at a distance of 2 mm from the rivet rows and half way between the rivet columns.

The regions of the most severe stress concentration which are of primary concern for fatigue are located beneath the rivet heads and at the faying joint surface, in either case hidden from the capabilities of conventional experimental stress analysis techniques. These critical areas are, however, accessible for numerical analyses. For the lap joint configuration considered in the FE analyses by Rans et al. [7], the neutral line model by Schijve was found to provide accurate predictions of secondary bending only up to a distance of three rivet diameters from the rivet row centre line. More near the hole the simple model proved inaccurate due to significant variations in secondary bending along the joint width.

Altogether, the available literature evidence cited in this section suggests that the model of Schijve can produce reliable estimates of nominal bending stresses for riveted joints with eccentricities.

Das et al [5] provided favourable comparisons between the strain gauge readings, 3-D FE results and local stresses computed based on the nominal bending stresses derived from their simple model for a padded riveted lap joint.

5. Effect of secondary bending on the fatigue performance of riveted joints

Fatigue tests of Hartman and Schijve [3] were conceived to investigate the dependence of the riveted joint fatigue performance on the amount of secondary bending. The geometry and dimensions of their specimens are shown in Fig. 9. Differences in the k_b -factors for the two series of lap joints (A and B, Fig. 9) were introduced by varying the rivet row spacing. The differences for the single strap joints (C, D and E, Fig. 9) were obtained by varying the number and the thicknesses of the straps. A symmetrical double strap joint (F, Fig. 9) for which secondary bending does not occur served as a reference case. Measures were taken by the authors to make the differences in the fatigue behaviour of the specimens stem mainly from the differences in the amount of secondary bending. With this end in view, all specimens were cut from the same batch of the material (2024-T3 Alclad) and the rivet

type, the rivet diameter (D_0) and the rivet driven head diameter, $D = 1.5D_0$, were the same for all specimens.

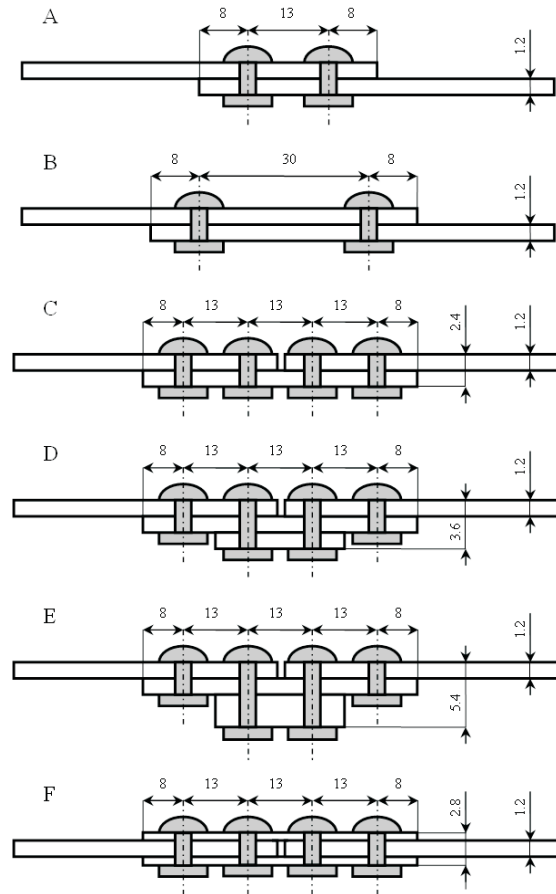


Fig. 9. The geometry and dimensions of the riveted specimens tested by Hartman and Schijve [3]

The S_b vs. S dependence for each specimen can be derived utilizing the neutral line model of Schijve [4]. The model application to the lap joint has already been considered earlier in this paper, see also Fig. 1. As said previously, for the type A and B configuration from Fig. 9, the maximum bending stresses and, at the same time, the maximum total tensile stress ($S + S_b$), where S is computed for the local sectional area neglecting the rivet holes, always occur at the outer rivet rows (location A and B in Fig. 1). The deflected neutral axis of a single strap joint and the division of the joint into three segments is schematized in Fig. 10. Due to the joint symmetry it is enough to only consider half of the configuration. The bending stresses were computed at four sections (α, β, γ and δ) shown in Fig. 10. For specimen C and D, the critical locations where the highest total tensile stresses occur are

at the inner rivets (section δ , Fig. 10). This holds also true for specimen E at $S \leq 25$ MPa, but for larger applied stress levels the critical location shifts to section α . Because all constant amplitude fatigue tests of Hartman and Schijve were carried out at the same applied mean stress of 70 MPa, the above implies that at the maximum of a fatigue cycle the peak total tensile stress ($S + S_b$) in specimen E always occurred in section α . At the same time, the total stress amplitude $(S + S_b)_a$ was always higher for section α than for section δ .

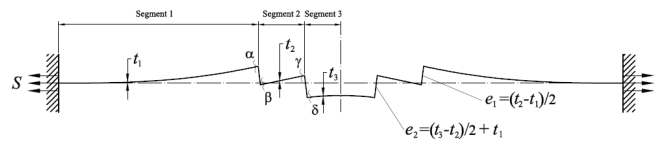


Fig. 10. The deflected neutral line and the division into segments for a single strap joint

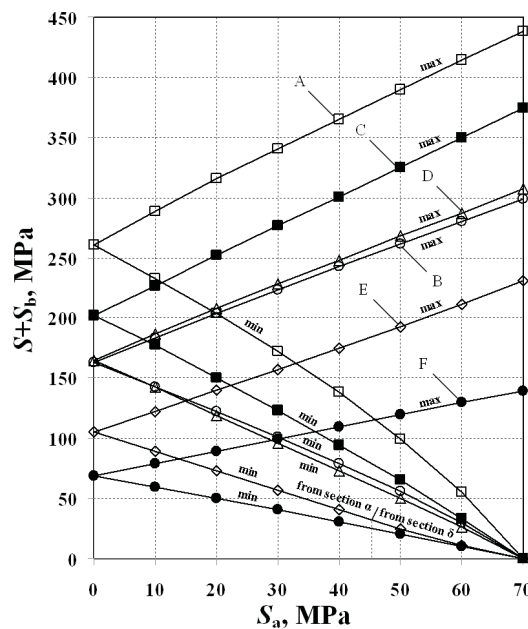


Fig. 11. The computed according to Schijve’s model peak total stress at the critical rivet row against the applied stress amplitude for the specimens from Fig. 9

Plots in Fig. 11 show the peak total tensile stress at the critical location calculated at the maximum (notation “max”) and at the minimum (notation “min”) of a fatigue cycle presented against the applied stress amplitude S_a . For specimens A, B, C and D the fatigue crack nucleation sites observed by Hartman and Schijve on the specimen fracture surfaces agree with the locations of the computed maximum tensile stresses. With specimens E,

however, only at the highest applied stress amplitudes ($S_a \geq 56$ MPa) the failure changed over from the longer strap (section δ , Fig. 10) to the sheet at the outer rivet row (section α). Such a behaviour can hardly be linked with the bending stress performance described above.

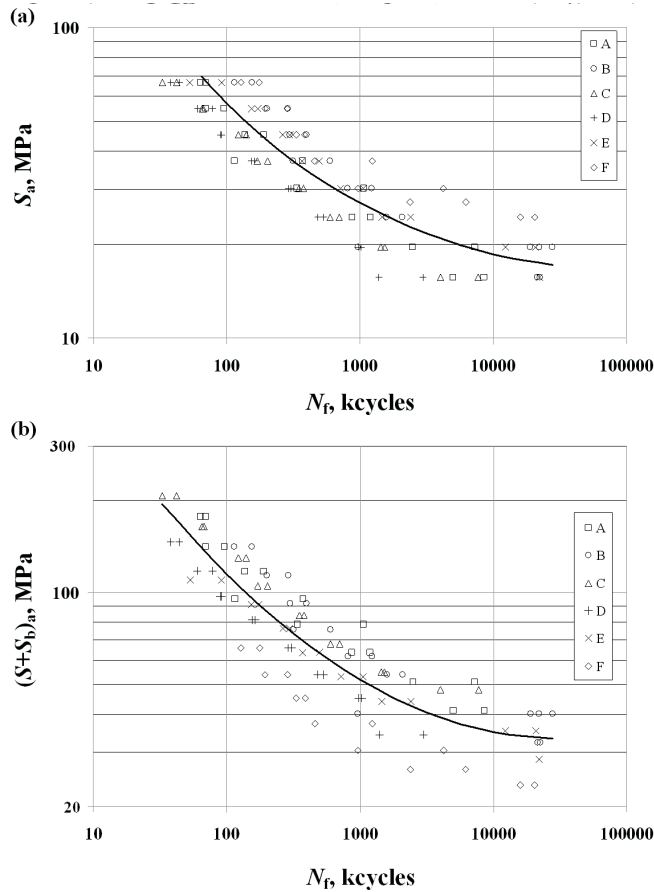


Fig. 12. Correlation between the fatigue lives observed in test by Hartman and Schijve [3] and: (a) the applied stress amplitude; (b) the peak total stress amplitude

In Figs 12a and b, the observed fatigue lives (N_f) for all specimens are correlated in terms of the applied stress amplitude S_a and the total stress amplitude $(S + S_b)_a$. Also shown are the corresponding trend lines. Equally large scatter in the data points is seen for both ways of the presentation. If the joint endurance were only dependent on $(S + S_b)_a$, then taking into account that $S_b=0$ for specimen F the following equation should be satisfied for a given fatigue life

$$(\check{S} + S_b)_{a,SB} = S_{a,F} \tag{16}$$

where the subscript SB refers to any specimen for which secondary bending occurs.

Shown in Fig. 13 by the dashed lines are the \check{S}_a vs. N_f plots for all specimens with eccentricities ensuing from Eq. (16). S_b is computed from Schijve's model and $S_{a,F}$ comes from the trend line representing the fatigue test results for specimens F. The actual mean curves S_a vs. N_f for the other specimens are also presented in Fig. 13 as the full lines. Evidently, the predicted from Eq. (16) reduction in the fatigue strength due to the secondary bending is larger than observed because for every specimen the \check{S}_a vs. N_f curve falls significantly below the S_a vs. N_f curve.

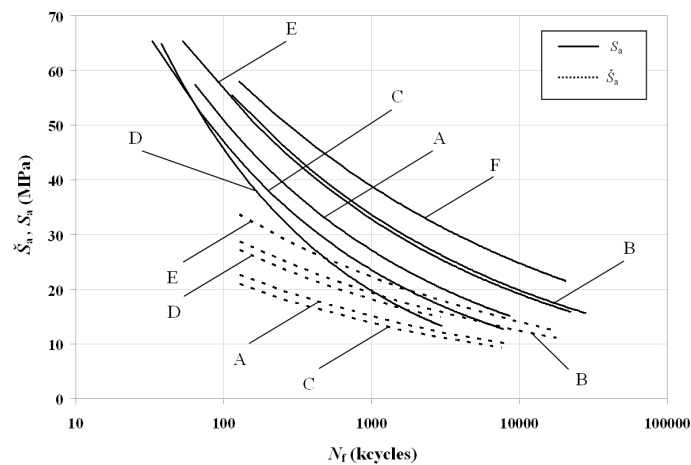


Fig. 13. Comparisons between the actual and computed using model [4] mean $S - N$ curves for the specimens with eccentricities

Altogether, the results presented in Figs 12 and 13 imply that the $(S + S_b)_a$ parameter is not capable of consolidating the data points for specimens of various configurations along a single $S - N$ curve and leads to an overestimate of secondary bending detrimental effects on the joint fatigue properties. Even qualitatively some misjudgments are obtained since, according to the fatigue tests, the order of joints with decreasing fatigue strength is F, B/E, A, C, D whilst, according to the increasing k_b value the order is F, E, B/D, A, C.

The lack of correlation between the calculated bending and the fatigue test results is not surprising since it is well known that the fatigue cracking of a notched component is controlled by the local stresses at the crack nucleation site rather than by the nominal stresses. As already said in the Introduction, the stress state near the rivet hole depends on a number of factors. Consequently, depending on a specific combination of the joint geometry, rivet material and type, sheet material and the riveting process the same nominal stress amplitude $(S + S_b)_a$ may be associated with different

local stress amplitudes. Certainly with the tests by Hartman and Schijve, the differences in the bending stresses are not the sole cause of the observed differences in the fatigue performance of their specimens. First, the load transmission is very different for the double strap joint (specimen F) compared to the single strap joints C, D and E. Moreover, within the latter joints the load transfer must have been also diversified due to the different strap numbers and thicknesses. Fatigue tests on riveted specimens indicate considerable fatigue life improvements due to increasing the rivet hole expansion (e.g. by applying a larger riveting force or by plastically expanding the hole prior to the rivet installation) and generating in this way a more beneficial residual stress field [2, 10]. At the same time, the experimental work by Müller demonstrates that the hole expansion becomes smaller for a larger sheet thickness in spite of the same driven head diameter [2]. With the experiments of Hartman and Schijve, the above implies that installing the rivets to obtain the same D/D_0 ratio for all specimens could lead to a diversification in the hole deformation depending on the joint total thickness. It can be concluded that only for specimens A, B and C both the load transmission and the residual stress field were very much alike. Consequently, only for these joints the differences in the fatigue behaviour can be fully attributed to secondary bending. The above reasoning is backed up by comparing the scatter of the $S - N$ data for specimens A, B, and C. Whilst for the S_a vs. N_f presentation of the results the correlation coefficient is 0.87, its value jumps up to 0.96 when the fatigue life is correlated using $(S + S_b)_a$.

A question arises about the significance of the simple models [4,5] for predictions on the fatigue life of riveted joints. Only a semi-empirical prediction approach, like for example the concepts by Das et al [5] or by Homan and Jongebreur [11], is possible because it would be not feasible to account analytically for all the influences involved. Both methods referred to above are based on a similarity principle, namely it is assumed that the same local stress amplitude at the critical location for two different riveted joints yields the same fatigue life. The predictions for the actual joint are extrapolated from a known $S - N$ curve for a so called reference riveted joint. The approach requires calculation of the peak local stress for the actual riveted joint and for the reference joint. This local stress level can be approximated by the superposition of three components, namely the stresses induced by the bypass load, the transfer load** and secondary bending. Each stress component is expressed as the product of the nominal stress and

** Bypass load is the part of the load passing the rivet hole, i.e. remaining in the sheet; transfer load is the part of the load transmitted by the rivet to another sheet.

the appropriate stress concentration factor. The experimental verification of models [4,5] in the literature, as considered earlier in this paper, allows of an opinion that these simple concepts may provide easy means to reliably estimate the nominal stress induced by secondary bending for a given riveted joint configuration.

6. Conclusions

1. Load path eccentricity in lap and single strap riveted joints causes bending moments under nominally tensile loading conditions. Due to the above phenomenon referred to as secondary bending significant bending stresses are induced. For the lap joints, the peak bending stresses always occur at the outer rivet rows.
2. The amount of secondary bending can be estimated by simple theoretical models developed by Schijve and by Das et al. According to either model, the joint region is considered as an integral beam and, hence, the presence of the middle rivet rows as well as the inhomogeneous load transmission through the sheets within the overlap area is not accounted for.
3. Differences between the results from both models become significant for thinner sheets and tend to vanish when the sheet thickness increases. The main reason for the discrepancies is a different description of the overlap deflections inherent in either model.
4. From either model, the bending factor is a nonlinear function of the applied stress level. The severity of bending increases for thicker sheets and diminishes with increasing the spacing between the rivet rows.
5. From reported in the literature comparisons between simple model results, strain gauge measurements and finite element analyses it can be concluded that the models provide reliable estimates of the nominal bending stresses at critical rivet rows.
6. The unsatisfactory correlation between the simple model results and the observed fatigue lives for riveted joints with eccentricities stems from disregarding by the simple models factors which, in addition to secondary bending, can affect the fatigue behaviour of riveted joints.
7. Bending factors estimated using the simple models can be utilized in currently used semi-empirical concepts for predictions on the fatigue life of riveted joints.

The authors acknowledge a financial support from the Eureka project No. E!3496.

Manuscript received by Editorial Board, September 01, 2008;
final version, November 25, 2008.

REFERENCES

- [1] Schijve J.: Fatigue life until small cracks in aircraft structures. Durability and damage tolerance. Proc. FFA/NASA Int. Symp. on Advanced Structural Integrity Methods for Airframe Durability and Damage Tolerance., Hampton, Virginia, 1994, Harris C.H. ed., Part 2, Publ. No. 3274, pp.665-681.
- [2] Müller R. P. G.: An experimental and analytical investigation on the fatigue behaviour of fuselage riveted lap joints. The significance of the rivet squeeze force, and a comparison of 2024-T3 and Glare 3, Ph.D. Thesis, Delft University of Technology, 1995.
- [3] Hartman A., Schijve J.: The effect of secondary bending on the fatigue strength of 2024-T3 Alclad riveted joints, NLR TR 69116U, Amsterdam, 1969.
- [4] Schijve J.: Some elementary calculations on secondary bending in simple lap joints, NLR TR 72036, Amsterdam, 1972.
- [5] Das G. K., Miller M., Sovar T.: Durability assessment of fuselage single shear lap joint with pads, Proc. of the 21st Symposium of the International Committee on Aeronautical Fatigue (ICAF' 2001), Design for Durability in the Digital Age, Ed. J. Rouchon, Toulouse, France, June 27-29, 2001, Vol. I, pp.567-595.
- [6] Skorupa M., Korbel A., Machniewicz T.: Analysis of secondary bending for riveted joints with eccentricities, Bulletin of the Military University of Technology, Warsaw, Accepted for publication in 2009 (in Polish).
- [7] Rans C. D., Straznicky P.V., Alderliesten R.C.: Effects of Rivet Installation on Residual Stresses and Secondary Bending Stresses in a Riveted Lap Joint, Proc. of 48th AIAA/ASME/ASCE/AHS/ASC Structures, Structural Dynamics, and Materials Conference, Waikiki, Hawaii, 2007.
- [8] De Rijck R.: Stress analysis of fatigue cracks in mechanically fastened joints, Ph.D. Thesis, Delft University of Technology, 2005.
- [9] Brenner L., Hübsch B.: Lebensdauer-Untersuchungen an Nietverbindungen, Report EF30 – TB 8, Dornier, Friedrichshafen, 1969.
- [10] Rodman G. A., Creager M.: Split mandrel vs spleet sleeve coldworking: dual methods for extending the fatigue life of metal structures. Proc. of FAA/NASA Int. Symp. of Advanced Structural Integrity Methods for Airframe Durability and Damage Tolerance, 4-6 May 1994, Hampton, VA, NASA-CP-3274, pp.1078-1086.
- [11] Homan J. J., Jongebreur A.A.: Calculation method for predicting the fatigue life of riveted joints. Proc. of the 17th Symposium of the International Committee on Aeronautical Fatigue (ICAF 1993), Durability and Structural Integrity of Airframes, Ed. A.F. Blom, Stockholm, 1993, Vol. I, pp.175-190.

Modelowanie wtórnego zginania w nitowych połączeniach z mimośrodem

Streszczenie

W artykule rozważono dwa proste teoretyczne modele zaproponowane w literaturze do analizy tzw. wtórnego zginania występującego w połączeniach nitowych z mimośrodem poddanych rozciąganiu. Modele te zostały zaimplementowane w programach komputerowych i zastosowane do określenia wpływu wybranych parametrów konstrukcyjnych połączenia nitowego oraz poziomu obciążenia na naprężenia wywołane wtórnym zginaniem. Wyniki uzyskane z wykorzystaniem

modeli oraz dostępne eksperymentalne i numeryczne dane literaturowe sugerują, że obie koncepcje umożliwiają poprawną ocenę nominalnych naprężeń zginających w krytycznym rzędzie nitów. Przeprowadzone analizy wykazują, że odnotowaną w literaturze redukcję wytrzymałości zmęczeniowej połączenia nitowego w zależności od jego konfiguracji geometrycznej można powiązać ze wzrostem wtórnego zginania. Pokazano, że niezadawalająca ilościowa korelacja pomiędzy wynikami przewidywanymi przy użyciu jednego z rozważanych modeli a trwałością obserwowaną w badaniach zmęczeniowych próbek nitowanych wynika z nieuwzględnienia w rozważanych koncepcjach nierównomiernego transferu obciążeń przez złącza, a także pominięcia wpływu procesu nitowania. Równocześnie stwierdzono, że omawiane tu proste modele są dogodnym narzędziem do oceny wpływu wtórnego zginania i mogą znaleźć zastosowanie we współcześnie stosowanych półempirycznych metodach przewidywania trwałości zmęczeniowej złączy nitowych.